



HAL
open science

Impact of alternative cementitious material on the mechanical and transfer properties of concrete

Alexandre Pavoine, David Harbec, Thierry Chaussadent, Arezki Tagnit-Hamou, Loïc Divet

► **To cite this version:**

Alexandre Pavoine, David Harbec, Thierry Chaussadent, Arezki Tagnit-Hamou, Loïc Divet. Impact of alternative cementitious material on the mechanical and transfer properties of concrete. *Materials Journal*, 2014, 111 (3), pp 251-261. hal-01004231

HAL Id: hal-01004231

<https://hal.science/hal-01004231>

Submitted on 11 Jun 2014

HAL is a multi-disciplinary open access archive for the deposit and dissemination of scientific research documents, whether they are published or not. The documents may come from teaching and research institutions in France or abroad, or from public or private research centers.

L'archive ouverte pluridisciplinaire **HAL**, est destinée au dépôt et à la diffusion de documents scientifiques de niveau recherche, publiés ou non, émanant des établissements d'enseignement et de recherche français ou étrangers, des laboratoires publics ou privés.

1 **IMPACT OF ALTERNATIVE CEMENTITIOUS MATERIAL ON THE**
2 **MECHANICAL AND TRANSFER PROPERTIES OF CONCRETE**

3

4 Alexandre Pavoine, David Harbec, Thierry Chaussadent, Arezki Tagnit-Hamou and Loïc
5 Divet

6 **Biography:**

7 **Alexandre Pavoine** is Head of the Eco-material laboratory in the Technical Research Center
8 of the region of Ile-de-France (France). He received his PhD in materials sciences from the
9 University of Paris. The subject of his PhD thesis was the risk of development of Delayed
10 Ettringite Formation in concretes. His research interests include durability of concrete and the
11 development of alternative materials for concrete.

12

13 **David Harbec** is Professional Researcher at the Researcher Center on Concrete
14 Infrastructures (CRIB) of the Université de Sherbrooke. He received his PhD in Chemical
15 Engineering from McGill University. His research interests include synthesis, microstructure
16 and physical chemistry study and characterization of nanometric cementitious materials and
17 alternative supplementary cementitious materials.

18

19 **Thierry Chaussadent** is a senior researcher in the French institute of science and technology
20 for transport, development and networks (IFSTTAR, Paris, France). His researches focus on
21 the sustainability of reinforced concrete and more particularly on corrosion and protection of
22 steel reinforcement.

23

24 **Arezki Tagnit-Hamou** is Professor at the Department of Civil Engineering of the Université
25 de Sherbrooke and Fellow of ACI. He is involved in various research topics including

1 physico-chemistry and microstructure of cement and concrete, supplementary cementitious
2 materials, and sustainable development. He is member of Board Advisory Committee on
3 Sustainable Development (BAC-SD) and committee C555 - Concrete with Recycled
4 Materials.

5

6 **Loic Divet** is Deputy Head of Materials Department at IFSTTAR (Paris – France). He has
7 over 25 years relevant experience, involving mainly in the engineering of construction
8 materials including concrete, mortar, stone and brick-built masonry. His research interests
9 include concrete pathology and the development of alternative materials for cement and
10 concrete.

11

12

ABSTRACT

13 An experimental program was carried out to characterize the risk of corrosion in reinforced
14 concretes, designed with alternative cementitious materials (ACMs). The study focuses on
15 three alternative cementitious materials used with ordinary Portland cement: glass powder
16 (GP) obtained from mix glass, alternative fly ash (AFA) obtained from the combustion of
17 wastepaper deinking sludge and wood residues in a fluidized-bed reactor, and limestone filler
18 (LF). Concrete specimens casted with a Water-to-Binder ratio (W/B) of 0.4 and 0.55 were
19 tested in order to determine compressive strength, chloride ion penetration, chloride diffusion,
20 and porosity accessible to water. Reinforced concretes were also submitted to accelerated
21 corrosion tests. The use of GP in replacement of cement yielded to a good resistance to
22 chloride ion penetration. In this case, low level of chloride ion penetration is maintained
23 despite the increase of W/B. Hence, measurements of chloride ion penetration do not
24 correlate with compressive strength values. The AFA slightly increases the chloride ion

1 penetration, while the use of limestone filler has no significant impact. The chloride ion
2 penetration tests show a good relation with the accelerated corrosion tests.

3

4 **Keywords:** alternative cementitious materials, glass powder, alternative fly ash, limestone
5 filler, corrosion, chloride, concrete durability, concrete transfer properties.

6

7

INTRODUCTION

8 Damages caused by the corrosion of steel are the main cause of premature deterioration of
9 reinforced concrete structures. In the United States, the annual cost of repair in 2002 was
10 evaluated to 271 million dollars¹. The risk of corrosion of steel is mainly associated with
11 either the penetration of chloride ions and/or a decrease of the pH induced by carbonation of
12 the binder. The use of supplementary or alternative cementitious materials (ACMs) to replace
13 Ordinary Portland Cement (OPC) is often required to achieve low chloride ion penetration
14 and durable concretes. The impact of fly ash (FA), silica fume (SF) and ground granulated
15 blast furnace slag (GGBFS) in a binary or a ternary system with OPC has been extensively
16 studied²⁻¹¹. Pozzolanic materials are known to react slowly with calcium hydroxide, resulting
17 from OPC hydration or already present within the added materials. Finely divided Calcium
18 Silicate Hydrates (C-S-H) with lower CaO/SiO₂ ratio (C/S) are formed and fill the fine
19 porosity¹². Limestone used in blended cements also has a chemical effect that contributes to
20 the acceleration of calcium silicate hydration by the formation of carboaluminate phases¹³⁻¹⁴.
21 Combined with the chemical effect, fine particles added to cement, especially limestone filler,
22 can also provide nucleation sites to form first hydrates and thus accelerate the hydration¹⁵⁻¹⁶.
23 These additional gels contribute to a densification of the microstructure and increase the pore
24 network tortuosity² and mechanical properties. Pozzolanic materials reduce the chloride ion
25 penetration by modifications of the cement paste microstructure and the nature of C-S-H

1 formed. The impact of limestone filler on concrete resistance towards chloride penetration is
2 complex. Additional negative effects may be attributed to the diluting effect of clinker, the
3 presence of a porous and connected paste-aggregate transition zone, the higher level of OH⁻
4 in the porous solution¹⁷, and the decrease of the ability of chloride binding into
5 carboaluminate phases¹⁸. Nevertheless, the use of limestone blended Portland cement can
6 improve the durability compare to OPC¹⁴.

7 ACMs are also developed to offer new opportunities to decrease the environmental impact of
8 concrete and contribute to the valorization of industrial by-products. This paper relates on
9 results obtained on casted concretes with a glass powder (GP) obtained by finely crushing
10 mix glass bottles, an alternative fly ash (AFA) coming from the combustion of wastepaper
11 de-inking sludge and wood residues in a fluidized bed for the co-generation of electricity, and
12 a limestone filler (LF) as a limestone blended cement. The properties of these concretes are
13 compared to those of OPC concretes.

14 Finely ground GP has a pozzolanic activity¹⁹⁻²¹. In terms of reactivity and impact on the
15 concrete durability, the properties of GP are often compared to those of class F fly ash²². Its
16 high fineness removes all risks of swelling reaction by alkali-silica reaction in concretes
17 when mixed with reactive aggregates²³. AFA can have hydraulic activity, due to the presence
18 of free lime, and pozzolanic activity, due to the presence of aluminosilicate materials that can
19 react with calcium hydroxide²⁴. If ACMs can contribute to a densification of the binder
20 matrix, the cement dilution and/or pozzolanic activity can reduce the resistance to
21 carbonation. As a consequence of these contrary effects, the impact of ACMs on concrete
22 durability is complex^{6,9,25}. The specific impact of the studied ACMs on concrete durability
23 must be evaluated to promote these new materials for appropriate environmental conditions
24 for concrete structures.

RESEARCH SIGNIFICANCE

The mechanical properties of concretes made with ACMs are often well characterized but the risk of steel corrosion is generally not deeply studied. The work carried out in this investigation describes an accelerated corrosion test that allows characterizing both the periods of initiation and propagation of steel corrosion in concrete. Meanwhile, it correlates the impact of three ACMs to the chloride ion penetration and the risk of corrosion of reinforced concretes. Also, this research illustrates the independence between concrete mechanical properties and durability.

EXPERIMENTAL PROCEDURE

The experimental design includes eight concrete mixes. The latter consist of four different binders (OPC as control, OPC substituted with 20% of GP, OPC substituted with 20% of AFA, and a 10% limestone filler blended OPC (LF)). The rate of 20% for the substitution of OPC by GP and AFA corresponds to an optimal dosage obtained in previous works based on the monitoring of mechanical properties and permeability with curing time²⁶. The LF cement is a common commercial cement that is used in this study in order to compare its properties with the other additions (AFA and GP) and OPC. Each binder is mixed using two water-to-binder ratios (W/B: 0.4 and 0.55). For each batch, specimens were cured in a 100% relative humidity room for a time depending of each specific test procedure. Concrete specimens are tested for compressive strength, chloride ion penetration²⁷ and porosity accessible to water²⁸. An accelerated corrosion test has been implemented and conducted to evaluate the behavior of reinforced concretes in a rich chloride environment.

Materials

The physical properties and chemical analysis of GP, AFA, LF and OPC are shown in Table 1 and their particle size distribution, in Fig. 1. X-ray diffraction analysis for GP and AFA have shown that GP is a totally amorphous product while AFA is composed of calcium oxide

1 (CaO), calcium carbonate (CaCO_3), anhydrite (CaSO_4) and gehlenite ($\text{Ca}_2\text{Al}_2\text{SiO}_7$) as main
2 crystalline phases.

3 Trial using the modified Chapelle test²⁹ confirmed that GP has a pozzolanic activity. The
4 pozzolanicity of GP was also verified by monitoring in cement pastes the decrease of the
5 portlandite peak using X-ray diffraction³⁰. The capacity of consumption of calcium hydroxide
6 by GP is estimated to 418 grains $\text{Ca}(\text{OH})_2/\text{oz}$ (955 $\text{mgCa}(\text{OH})_2/\text{g}$). AFA has both a
7 pozzolanic activity and hydraulic activity. Determined by the modified Chapelle test²⁹, AFA
8 is able to react with 36 grains $\text{Ca}(\text{OH})_2/\text{oz}$ (82 $\text{mg Ca}(\text{OH})_2/\text{g}$). Taking into account of the
9 9.2% of free lime initially present in AFA, the capacity of consumption of $\text{Ca}(\text{OH})_2$ by AFA
10 is estimated to around 89 grains $\text{Ca}(\text{OH})_2/\text{oz}$ (204 $\text{mg}(\text{Ca}(\text{OH})_2)/\text{g}$).

11 One siliceous sand and two crushed coarse limestone aggregates were used for concrete
12 mixes which are summarized in Table 2. An air-entraining admixture (in a range of 0.46 to
13 0.89 oz/lb of binder (29.0 to 52.6 ml/100 kg of binder)) and a superplasticizer (in a range of
14 0.0 to 0.3 oz/gal of concrete (0.0 to 2.2 l/m^3) have been used to achieve an entrained air
15 content between 6% and 8% and an initial slump between 7.2 in. and 8.8 in. (180 and 220
16 mm). This air content range is normally indicated in Canadian specifications.

17 **Specimens**

18 Concrete cylinders of diameter 3.94 in. (100 mm) and length 7.87 in. (200 mm) were used to
19 investigate the compressive strength, chloride ion penetration and porosity accessible to water.

20 **Accelerated corrosion test**

21 The experimental setup designed for the accelerated corrosion test is illustrated in Fig. 2. It
22 consists of four concrete elements (39.4 in.(100 cm) long, 3.94 in. (100 mm) thick and 7.87 in.
23 (200 mm) high) sealed together to form a closed container of 51.5 U.S gallons (195 liters) of
24 saline solution (NaCl 5%). Each side of the structure is built with a different reinforced
25 concrete with three series of three bars (\varnothing 0.39 in. (10 mm)) distant of 3.94 in. (100 mm) and

1 placed at 7.87, 13.8 and 19.7 in. (20, 35 and 50 mm) from the internal side in contact with the
2 saline solution. Each bar is 9.8 in. (250 mm) long. The extremity of the bars is coated with
3 epoxy to control the surface (4.87 in². 31.4 cm²) of steel in contact with the concrete and
4 avoid interferences created by the extremity of concrete (air, cracks, liquid flow). A constant
5 difference of electrical potential of 5V is imposed between each steel bar and a galvanized
6 steel grid placed at around 2 in. (5 cm) from the concrete. A resistance (1Ω) placed in each
7 electric circuit allows monitoring the current in each bar via the measurement of voltage.

8 **ITEMS OF INVESTIGATION**

9 • *Compressive strength test*

10 Compressive strength tests are conducted in accordance with ASTM C39³¹ on cylinders kept
11 in a 100% relative humidity room for 1, 7, 14, 28, and 91 days.

12 • *Rapid chloride ion penetration test*

13 The tests of rapid chloride ion penetration are conducted according to the procedure
14 described in ASTM C1202²⁷.

15 • *Chloride ion penetration test*

16 This test is conducted accordingly to the French association of Civil Engineering
17 recommendations (AFGC)²⁸. It was performed on three concrete cores of 1.97 in. (5 cm)
18 thickness taken from cylinders for each concrete. After 91 days curing, specimens were
19 saturated with a basic solution, NaOH (0.025 mol/l) + KOH (0.083 mol/l), under vacuum
20 during 20 hours. Concrete cores are then placed between two cells. One cell contains a 3%
21 NaCl solution (cathode side) and the other, a 0.3N NaOH solution (anode side). A 30V
22 potential difference is applied between the two cells at 68°F ± 1.8°F (20 ± 1°C). Chloride ion
23 penetration is expressed by the electric charge in Coulombs passing through the core during 6
24 hours of testing.

1 The migration depth (X_d) is obtained by a pulverization of 0.05 molar silver nitrate (AgNO_3)
2 on fresh broken samples. The non-stationary diffusion coefficient (D_{app} m^2/s) is obtained
3 with:

$$4 \quad D_{app} = \frac{R.T.L}{z.F.\Delta E} \cdot \frac{(X_d - \alpha.\sqrt{X_d})}{\Delta t}$$

$$5 \quad \text{Where } \alpha = 2\xi\sqrt{\frac{R.T.L}{Z.F.\Delta E}} \text{ and } \xi = \text{erf}^{-1}\left(1 - 2 \times \frac{c_d}{c_0}\right)$$

6 R = the gas constant ($R = 8.3144 \text{ J.mol}^{-1}.\text{K}^{-1}$); T = the absolute temperature (K); L =
7 specimen's thickness (m); z = the valence ion ($z = 1$); F = the Faraday constant ($F = 96480$
8 J.V^{-1}); ΔE = the potential drop between the surfaces of specimen (V); Δt = test's duration (s);
9 X_d = chloride depth, c_0 = the chloride concentration of the catholyte solution (upstream
10 compartment) in mol.L^{-1} and C_d = chloride threshold concentration detected by colorimetry in
11 mol.L^{-1} ($C_d = 0.07$). For $C_0 = 0.5 \text{ mol.L}^{-1}$, $\zeta = 0.764$.

12 • *Accelerated corrosion test*

13 This test is conducted on concrete structures as described above. The concrete specimen are
14 demolded 48 hours after their fabrication and cured in a 100% relative humidity at 68°F
15 (20°C) for 6 weeks. Electronic devices are connected during the 7th week on the superficially
16 air dried concretes at 68°F (20°C). The 8th week, the concrete structure is filled with tap water
17 to saturate the concrete and check the tightness and liquid leaks. The 9th week, tap water is
18 replaced by a saline solution (5% NaCl) and a potential difference of 5V is applied between
19 the cathode (galvanized steel grid placed in saline solution) and the anode (each 36 bars
20 tested). For each steel bar, the voltage is periodically measured on a 1Ω resistor connected in
21 between the cathode and the anode. The measurements are thereafter converted into electrical
22 current data using the Ohm's law.

23 To investigate the microstructure at the end of the accelerated corrosion tests, the corrosion
24 products developed in the four concretes (OPC, GP, AFA, LF) mixed at a W/B=0.55 were

1 observed using SEM and analyse using energy-dispersive spectroscopy (EDS). In this sense,
2 corroded concrete samples were cored around the reinforcing bars and fresh factures pieces
3 were taken from each core samples for SEM observations. The SEM acceleration voltage and
4 emission current were respectively set to 15.0 kV and 60 μ A. Complementary to these
5 microscopic investigations, corroded bars have been extracted from the four concretes (W/B
6 = 0.55) in order to evaluate the loss of mass during the test.

7 • *Porosity accessible to water*

8 This test is conducted accordingly to the AFGC recommendations²⁸. Three concrete cores (3
9 cm thickness) taken from cylinders are maintained under vacuum during 4 hours and then
10 saturated under vacuum by tap water during 20 hours. Saturated samples are weighed in air
11 (M_{air}) and in water (M_{water}). Concrete samples are then air dried at 224°F (105°C) up to
12 constant mass (M_{dry}). The accessible porosity to water (ϵ) is obtained by:

13
$$\epsilon(\%) = \frac{M_{air} - M_{dry}}{M_{air} - M_{water}} * 100\%$$

14

15 **EXPERIMENTAL RESULTS AND DISCUSSION**

16 **Compressive strength**

17 Compressive strengths of concrete at 1, 7, 14, 28, and 91 days are shown in Fig. 3 and 4 for
18 W/B of 0.4 and 0.55 respectively. After one day, the control concrete (OPC) exhibits the
19 highest compressive strength. After 7 days, LF concretes attained similar compressive
20 strength as the control. As previously shown³², the compressive strength of 20% AFA
21 concretes after 7 days is higher than that of the control. Filler effect of LF accelerates the
22 hydration of concretes with a high W/B ratio, probably by offering nucleation sites in a more
23 diluted system. The high reactivity of AFA at early ages can be explained by its fineness that
24 may accelerate its hydraulic activity. GP concrete has the lowest compressive strength at

1 early ages but the difference with the control concrete decreases with time due to the
2 pozzolanic activity of the GP. After 91 days, control and GP concretes have a similar
3 compressive strength.

4 For W/B=0.4, the dilution of Portland cement with limestone filler conducts to a significant
5 decrease of the compressive strength of -1174.7 psi (-8.1 MPa) after 91 days. No difference is
6 observed for a W/B ratio of 0.55. The compressive strength of LF concretes after 7 days of
7 maturation is similar to that of OPC concretes. It may be explained by both: the nucleation
8 sites offered by LF and, the higher fineness of the LF binder.

9 **Chloride ion penetration**

10 The results of rapid chloride ion penetration tests results are illustrated in Fig. 5 (W/B=0.4)
11 and 6 (W/B=0.55). After 28 days, the electrical indications of the tested concretes (in
12 Coulombs) to resist chloride ion penetration are similar for both W/B 0.4 and 0.55. For W/B
13 of 0.4, the electrical charges oscillated around the acceptable high limit by the standard
14 (4236 ± 631 Coulombs), while, they are in the upper limit for W/B 0.55 (5619 ± 1061
15 Coulombs). For a W/B ratio of 0.55, the electrical charges of AFA, LF and OPC concretes
16 are comparable and never achieve the moderate domain comprised between 2000 and 4000
17 Coulombs. GP concrete exhibits the most important decrease of chloride ion penetration after
18 28 days. After 91 days, the chloride ion penetration of this binder is more than the half of the
19 other tested binders. The great influence of GP on the reduction chloride ion penetration
20 reduction is accentuated with the increase of the W/B ratio. After 91 days, the GP chloride
21 ion penetration with W/B ratio of 0.55 (1313 ± 139 Coulombs) is more than the third of the
22 other tested binders.

23 Nominal particle size is an important parameter to control the reactivity of GP¹⁹, but some
24 other factors, such as glass content may be considered. After 220 days, Shayan and Xu²⁰

1 obtained a higher chloride ion penetration than what we obtained at a shorter time. Chloride
2 ion penetration can be reduced by increasing the GP proportion up to 30% of OPC content²⁰.
3 For a W/B ratio of 0.55, the use of AFA has an impact on the chloride ion penetration. Indeed,
4 it allows achieving the moderate domain comprised between 2000 and 4000 Coulombs. The
5 capacity of AFA to reduce the chloride ion penetration is less important than that of standard
6 FA, where a reduction of coefficient of chloride diffusion by more than 2 can be expected for
7 this grade of concrete⁵. Previous tests on concrete ages of 180 days and 1 year show that an
8 important decrease of the charge is expected in concrete with similar AFA³³.

9 Fig. 7 plots de chloride ion penetration in coulombs versus the coefficient of apparent
10 chloride ion diffusion (D_{app}). According to the test used, the obtained D_{app} are in a range of
11 high [$0-3.33E-12$ ft²/s ($0-3.09E-14$ m²/s)] and very high durability [>3.33 E-12 ft²/s ($3.09E-$
12 14 m²/s)]³³ whereas the electrical charges measured are in a larger scale from low to high
13 chloride ion penetrations²⁷. The comparison of these results reveals that from one side,
14 concretes can be separated from low to high chloride ion penetration and from the other side,
15 from high to very high durability. The tendency is that, when the chloride ion penetration
16 obtained by ASTM C 1202²⁷ increases, D_{app} also increases. This relation is not so clear for
17 concretes within the same range of durability. Within the high durability domain, the
18 electrical charge measured with ASTM standard can vary within a large scale (0-4000
19 coulombs) without influence on D_{app} . The test of ASTM C1202²⁷ and the criteria proposed to
20 evaluate chloride ion penetration appear to be more selective than those of the French method
21 proposed by AFGC²⁸.

22 **Corrosion test**

23 In Fig. 8, the evolution of current intensity in steel bars during the accelerated corrosion tests
24 are given for steel bars placed at 0.8 in. (20 mm) from the surface. This test gives interesting
25 data on the concrete behavior after the beginning of corrosion and more precisely the way it

1 performs against the stress induced by the formation of chlorinated iron oxides. The current
2 variation with time can schematically be described in three steps:

3 1) The current intensity decreases with time. This diminution can be explained by a
4 continuous penetration of chloride in the porosity toward the polarized steels. Salts may
5 precipitate within the porosity making the concrete progressively less penetrable by the
6 chloride ion and/or a protective oxide layers may be formed on the steel bars.

7 2) The current intensity remains constant. This step is not systematically observed. It is
8 generally encountered with steels placed deeper in the concrete. At this stage, we assume that
9 chlorides have reached the steel bars and the corrosion process begins. The evolution of the
10 microstructure of the concrete and its penetration of chloride ions remains unchanged with
11 time.

12 3) The current intensity increases and an important variation within the three steels placed at
13 the same distance from the surface can be recorded. This increase may be explained by a
14 degradation of concrete, due to the formation of expansive corrosion products, and of the
15 protective oxide layers on the steel bars. It may depend of the concrete resistance towards the
16 tensile stresses generated by the formation of corrosion products. The crack spread is
17 complex and can be greatly different between the three bars placed at the same distance from
18 the surface.

19 The test on the structure made with four concretes with a W/B ratio of 0.55 was stopped after
20 32 days because of large cracks causing major leaks of chloride solution.

21 The initial current measurements give information on concrete resistances. It can be clearly
22 observed that concretes with a W/B ratio of 0.55 have initial current intensity higher than
23 those measured on concretes with a W/B ratio of 0.4. According to the chloride ion
24 penetration measurements, the lowest initial currents are measured on concretes with GP.

1 One should also note that the initial intensity obtained for GP concretes and W/B ratio of 0.55
2 is lower than those measured on other concretes with a lower W/B ratio of 0.4.

3 This test gives information about the resistance to chloride ion penetration by the
4 determination of the duration before the corrosion is detected. In Fig. 8 for steels placed at
5 0.8 in. (20 mm) from the surface, the corrosion seems to begin rapidly. OPC, AFA and LF
6 concretes readily start with a higher initial current than the GP concrete: 8-10 mA for
7 W/B=0.4 concretes and 12-mA for W/B=0.55 concrete. currents increase (step 3) within the
8 seven first days for W/B=0.4, and within the first three days for W/B=0.55. The concretes are
9 immediately damaged after the beginning of the corrosion test. At W/B=0.4, it exists a period
10 of time when the current remains constant (step 2) after 7 days and the cracks development
11 provoke a sudden increase of the current intensity (step 3) with large variations. In the case of
12 the LF concrete, this occurs 15-20 days after the corrosion test was initiated. In the case of
13 the OPC and AFA concrete, this occurs 35-40 days after corrosion test was initiated.

14 For GP concretes, the current slightly decreases within the first five days (step 1) for
15 W/B=0.4 and slightly increase within the first seven days (step 3) for W/B=0.55. The current
16 remains constant afterwards (step 2) for both concretes. Similar observations can be drawn
17 from the monitoring of current intensity in bars placed at 1.4 in. (35 mm) from the surface of
18 the concrete.

19 Fig. 9 represents the time taken to detect corrosion at the end of step 1 for concretes with a
20 W/B ratio of 0.4 (Fig. 9a) and 0.55 (Fig. 9b). This time increases quasi-linearly with the
21 distance between the steel bars and the surface of concrete exposed to the saline solution.

22 This accelerated test of corrosion confirms the results obtained with the chloride ion
23 penetration tests. Indeed, GP concretes have high resistance to chloride ion penetration. The
24 use of this ACM with W/B=0.55 allows reaching similar resistance to chloride ion
25 penetration than that of the control concrete with W/B=0.4. The relative mass losses with

1 respect to the initial bar weight are given in Table 3 for bars initially placed at 20 mm from
2 the surface exposed to chloride solution.

3 Shayan and Xu.²⁰ show that the use of 20% GP in substitution of OPC does not have an
4 impact on the dynamic modulus of elasticity (E). The good behavior of GP concrete is not
5 thus explained by an increase of E. As it can be seen in Table 3, the quantities of corrosion
6 products are two to three times less important for GP concrete compares to OPC, LF and
7 AFA concretes. After 32 days of testing, the better resistance of GP concretes to the
8 generation of cracks may be explained by lower quantity of corrosion products. The lower
9 quantity of corrosion products thus exercises less tensile strength on the concrete.

10 **Porosity accessible to water**

11 The porosity accessible to water obtained by applying the method recommended by AFGC²⁸
12 is represented in Fig. 10. For concretes with W/B of 0.4, porosity varies closely between 13.0
13 and 15.1. The partial substitution of cement by 10% LF or 20% ACMs does not have a
14 significant impact after 91 days curing. The increase of W/B implies an increase of the
15 accessible porosity. OPC and 10% LF concretes show comparable porosity of 16.2% and
16 16.0% respectively. Contrary to concretes with W/B of 0.4, the substitution of cement by
17 20% ACMs in concretes with W/B of 0.55 resulted in an increase of porosity. Very high
18 values of 20.1% and 21.1% are obtained for AFA and GP.

19 There is no relation between the porosity accessible to water and the resistance to chloride
20 ion penetration and accelerated corrosion. Specifically for concretes with GP that have a
21 pozzolanic activity, the densification of the microstructure and the increase of the tortuosity
22 do not imply a decrease of porosity accessible to water. Attention should be paid to the fact
23 that the porosity accessible to water has a low degree of significance with the real transfer
24 properties of concrete.

25

1 SEM examination of concretes after corrosion test

2 The chloride ions (Cl^-) penetration during the accelerated corrosion tests notably initiates
3 reaction between Cl^- and Portlandite and weakens the protective hydroxide film on the steel
4 bars. These phenomena may also affect the microstructure and the hydration products, by
5 generating expansive corrosion products consisting of iron oxides (Fe_xO_y) and oxy-chloride
6 ($\text{Fe}_x\text{O}_y\text{Cl}_z$) around the steel bars³⁴.
7 Depending on its ability to resist to chloride ions penetration, concrete will develop different
8 morphologies of corrosion products with different Fe/Cl ratio. Thus, this ratio will decrease
9 with the increase of the chloride penetration and corrosion of the armature bars. While Fig.
10 11 to 14 present the morphology of the corrosion products and their respective EDS spectrum
11 obtained in four different concretes at the same W/B (OPC 0.55, 20% GP 0.55, 20% AFA
12 0.55, 10% LF 0.55). Table 4 summarizes the morphology type of the corrosion products
13 observed in each concrete and their respective Fe/Cl % atomic ratios. Empty cells means that
14 the associated corrosion product is not observed in the concrete.

15 1. OPC 0.55

16 Fig. 11 presents the morphology of the corrosion production and their respective EDS
17 spectrum observed in OPC 0.55. This concrete globally contains two types of corrosion
18 products: a) nested flower-like and b) lamellar-like corrosion products. These products show
19 a Fe/Cl ratios of 1.8 and 2.1 respectively. Petals in the flower-like products are 1 to 3 μm
20 wide, while the lamellae in the second products are 20 to 40 μm wide.

21 2. 20% GP 0.55

22 Fig. 12 presents the morphology of the corrosion production and their respective EDS
23 spectrum observed in 20% GP 0.55. This concrete mainly develops a gel-like corrosion
24 product. This product indicates a Fe/Cl of around 12.3.

25 3. 20% AFA 0.55

1 Fig. 13 exhibits the morphology of the corrosion production and their respective EDS
2 spectrum observed in 20% AFA 0.55. This concrete globally contains a) gel-like, b) globular-
3 like and c) hexagonal crystal-like corrosion products. These products indicate a Fe/Cl ratio in
4 the 1.3-2.2 range. As for 20% GP 0.55, the gel-like material is widely spread in the concrete
5 sample and the globular products show globules of 1 to 5 μm in diameter. The hexagonal
6 crystal-like products are $\approx 10 \mu\text{m}$ wide.

7

8 4. Binary OPC-LF concrete (LF 0.55)

9 Fig. 14 exhibits the morphology of the corrosion production and their respective EDS
10 spectrum observed in 10% LF 0.55. This concrete globally contains three different corrosion
11 products with the following morphologies: a) a gel-like and globular-like, b) nested needle-
12 like and c) lamellar-like corrosion products. These show a Fe/Cl in the 1.2-8.0 range. The
13 gel-like material and the nested needle-like product are widely spread in the concrete sample
14 and the globular products shows globules of 1 to 10 μm in diameter. Lamellae are 10 to 20
15 μm wide.

16 Globally, the Fe/Cl ratios in Table 4 agree with results obtained from the chloride ion
17 penetration and the accelerated corrosion tests, meaning that these ratios decrease with the
18 increase of the current intensity measured during the first and the second tests. 20% GP 0.55
19 concrete, which shows the lowest current value during both the chloride ions penetration and
20 accelerated corrosion tests, exhibits the least amount of corrosion products of product and the
21 highest Fe/Cl ratio values. OPC 0.55, 20% AFA 0.55 and 10% LF 0.55 concretes, which
22 show comparable results during both the chloride ions penetration and accelerated corrosion
23 tests, also indicate comparable low Fe/Cl ratios.

CONCLUSIONS

1
2 Besides their environmental impact, the use of ACMs brings additional mechanical and
3 durability properties to concrete. The present work illustrates that the use of these ACMs has
4 an impact on both the mechanical and transfer properties of concrete, such as the chloride ion
5 penetration and accelerated corrosion. At early ages (1 day), the dilution of OPC by ACMs
6 reduces the compressive strength. With time, concrete mixes designed with ACMs achieve
7 similar or greater compressive strengths than those attained by OPC concretes.
8 For the transfer properties, the replacement of 10% of OPC by LF or 20% of OPC by AFA
9 has no significant consequence on the resistance to chloride ion penetration. The pozzolanic
10 activity of GP decreases the chloride ion penetration of concrete. This effect is also observed
11 at high W/B.
12 The accelerated corrosion tests on reinforced concretes clearly show that concrete with 20%
13 GP exhibits a good resistance to the formation of corrosion products on steel bars, while the
14 other tested concretes are rapidly damaged using the same accelerated conditions.
15 Measurements of the porosity accessible to water show no relationship with the resistance to
16 chloride ion penetration and accelerated corrosion. Contrary to the chloride ion penetration
17 and acceleration corrosion tests, porosity accessible to water does not take into account the
18 tortuosity of the microstructure.

ACKNOWLEDGMENTS

19
20 The authors wish to express their acknowledgments to the Funds Research on Nature and
21 Technology of Québec and the French ministry of ecology for their financial support. They
22 also express their acknowledgments to Mr. Ablam Zidol and Mrs. Eleonore Mocaer for their
23 contribution to this study.

24

25

REFERENCES

1. Koch, G.H.; Brongers, M.P.H.; Thompson, N.G.; Virmani, Y.P., and Payer J.H., “Corrosion costs and preventive strategies in the United States”, *Supplement to Materials Performance*, July 2002, 11 p.
2. Li, S., and Roy; D.M., “Investigation of relations between porosity, pore structure, and Cl⁻ diffusion of fly ash and blended cement pastes”, *Cement and Concrete Research*, V. 16, 1986, pp. 749–59.
3. Song, H.-W., and Saraswathy, V., “Carbonation – Comparison of results for concretes containing PFA, cimentitious SLAG, or alternative aggregates”, *Materials Science and Technology*, V. 3, I. 2, 1986, pp.986-992.
4. Gjorv, O.E., “Effect of condensed silica fume on steel corrosion in concrete”, *ACI Materials Journal*, V. 92, I. 6, 1995, pp. 591-598.
5. Dhir, R.K., and Jones M.R., “Development of chloride-resisting concrete using fly ash”, *Fuel*, V. 78, 1999, pp. 137-142.
6. Osborne, G.J., “Durability of Portland blast-furnace slag cement concrete”, *Cement and Concrete Composites*, V. 21, I. 1, 1999, pp. 11-21.
7. Marcotte, T.D., “The influence of silica fume on the corrosion resistance of steel in high performance concrete exposed to simulated sea water”, *Journal of Materials Science*, V. 38, I. 23, 2003, pp. 4765-4776.
8. Thomas, M.D.A., and Matthews, J.D., “Performance of pfa concrete in a marine environment, 10-year results”, *Cement and Concrete Composites*, V 26, I. 1, 2004, pp. 5-20.
9. Song, H.-W., and Saraswathy, V. “Studies on the corrosion resistance of reinforced steel in concrete with ground granulated blast-furnace slag - An overview”, *Journal of Hazardous Materials*, V. 138, I. 2, November 2006, pp. 226-233.
10. Yuan, Q.; Shi, C.; De Schutter, G.; Audenaert, K., and Deng, D., “Chloride binding of

- 1 cement-based materials subjected to external chloride environment – A review”,
2 *Construction and Building Materials*, V. 23, 2009, pp. 1-13.
- 3 11. Cheewaket, T.; Jaturapitakkul, C., and Chalee, W. “Long term performance of chloride
4 binding capacity in fly ash concrete in a marine environment”, *Construction and Building*
5 *Materials*, V. 24, 2010, pp. 1352-1357.
- 6 12. Richardson, I.G., “The nature of C-S-H in hardened cements”, *Cement and Concrete*
7 *Research*, V. 29, I. 8, 1999, pp. 1131-1147.
- 8 13. Kakali, G.; Tsvivilis, S.; Aggeli, E., and Bati, M., “Hydration products of C₃A, C₃S and
9 Portland cement in the presence of CaCO₃”, *Cement and Concrete Research*, V. 30, I. 7,
10 2000, pp. 1073-1077.
- 11 14. Tsvivilis, S.; Chaniotakis, E.; Kakali, G., and Batis, G., “An analysis of the properties of
12 Portland limestone cements and concrete”, *Cement and Concrete Composites*, V. 24, I. 3-4,
13 2002, pp. 371-378.15.
- 14 15. Gutteridge, W.A, and Dalziel, J.A., “Filler cement: the effect of the secondary component
15 on the hydration of Portland cement: Part I. A fine non-hydraulic filler”, *Cement and*
16 *Concrete Research*, V.20, I. 5, 1990, pp. 778-782.
- 17 16. Bentz, D.P., “Modeling the influence of limestone filler on cement hydration using
18 CEMHYD3D”, *Cement and Concrete Composites*, V. 28, I. 2, 2006, pp 124-129.
- 19 17. Ghrici, M.; Kenai, S., and Said-Mansour, M., “Mechanical properties and durability of
20 mortar and concrete containing natural pozzolana and limestone blended cements”, *Cement*
21 *and Concrete Composites*, V. 29, I. 7, 2007, pp 542-549.
- 22 18. Ipavec, A.; Vuk, T.; Gabrovšek R., and Kaučič, V., “Chloride binding into hydrated
23 blended cements: The influence of limestone and alkalinity”, *Cement and Concrete*
24 *Research*, V.48, 2013, pp 74-85.
- 25 19. Shi, C.; Wu, Y.; Riefler, C., and Wang, H., “Characteristics and pozzolanic reactivity of

- 1 glass powders”, *Cement and Concrete Research*, V. 35, I.5, 2005, pp. 987– 993.
- 2 20. Shayan A., and Xu, A., “Performance of glass powder as a pozzolanic material a field
3 trial on concrete slabs”, *Cement and Concrete Research*, V. 36, I. 2, 2006, pp. 457–468.
- 4 21. Idir, R.; Cyr, M., and Tagnit-Hamou, A., “Pozzolanic properties of fine and coarse color-
5 mixed glass cullet”, *Cement and Concrete Composites*, V.33, I. 1, 2011, pp. 19-29.
- 6 22. Schwarz, N.; Cam, H., and Neithalath, N., “Influence of a fine glass powder on the
7 durability characteristics of concrete and its comparison to fly ash”, *Cement and Concrete
8 composites*, V. 30, I. 6, 2008, pp. 486-496.
- 9 23. Idir, R.; Cyr, M., and Tagnit-Hamou, A., “Use of fine glass as ASR inhibitor in glass
10 aggregate mortars”, *Construction and Building Materials*, V. 24, I. 7, 2010, pp. 1309–1312.
- 11 24. Bai, J.; Chaipanich, A.; Kinuthia, J.M.; O’Farrell, M.; Sabir, B.B.; Wild, S., and Lewis,
12 M.H., “Compressive strength and hydration of wastepaper sludge ash-ground granulated
13 blastfurnace slag blended pastes”, *Cement and Concrete Research*, Vol. 33, I. 8, 2003, pp.
14 1189-1202.
- 15 25. Ramezani pour, A.A., and Malhotra, V.M., “Effect of curing on the compressive
16 strength, resistance to chloride-ion penetration and porosity of concretes incorporating slag,
17 fly ash or silica fume”, *Cement and Concrete Composites*, V. 17, I. 2, 1995, pp. 125-133.
- 18 26. Zidol, A.; Pavoine, A., and Tagnit-Hamou, A., “Effect of glass powder on concrete
19 permeability”, International Congress on Durability of Concrete, Trondheim, Norway, 18-21
20 June 2012.
- 21 27. ASTM C1202 – 97, “Standard Test Method for Electrical Indication of Concrete's Ability
22 to Resist Chloride Ion Penetration”, ASTM International, West Conshohocken, PA, USA, 6
23 pages.
- 24 28. AFGC, “GranDuBé : Grandeurs associées à la Durabilité des Bétons”, *Presses Ponts et
25 Chaussées*, 2007, ISBN-10: 285978425X, 437 pages.

- 1 29. AFNOR NF P18-513., “Métakaolin, addition pouzzolanique pour bétons - Définitions,
2 spécifications, critères de conformité”, Mars 2010.
- 3 30. Harbec, D.; Tagnit-Hamou, A., and Gitzhofer, F. “Waste glass nanoparticles as an
4 alternative supplementary cementitious material”, 13th Int. Congr. Chem. of Cement, Madrid,
5 Spain, 3 to 8 July 2011, 626.
- 6 31. ASTM C39/C39M-03, “Standard Test Method for Compressive Strength of Cylindrical
7 Concrete Specimens”, ASTM International, West Conshohocken, PA, USA, 5 pages.
- 8 32. Xie, A.; Laldji, S.; Mikanovic, N., and Tagnit-Hamou, A. “Wastepaper Sludge Ash: A
9 New Type of Supplementary Cementitious Material Used in Concrete”, *XIII International*
10 *congress on the chemistry of cement*, Madrid, 3-8 July, 2011.
- 11 33. AFGC, “Conception des bétons pour une durée de vie donnée des ouvrages, Maîtrise de
12 la durabilité vis-à-vis de la corrosion des armatures et de l’alcali-réaction, État de l’art et
13 guide pour la mise en œuvre d’une approche performantielle et prédictive sur la base
14 d’indicateurs de durabilité”, juillet 2004, 252 pages (In French).
- 15 34. Koleva, D.A.; Hu J.; Fraaij, A.L.A.; Stroeven, P.; Boshkov, N., and de Wit, J.H.W.,
16 “Quantitative characterisation of steel/cement paste interface microstructure and corrosion
17 phenomena in mortars suffering from chloride attack”, V. 48, I. 12, *Corrosion science*, 2006,
18 pp. 4001-4019.
- 19
20
21
22
23

1
2
3
4
5
6
7
8
9
10
11
12
13
14
15
16
17
18
19
20
21
22
23
24
25

TABLES AND FIGURES

List of Tables:

Table 1 – Chemical and physical analysis of materials (% by mass)

Table 2 – Mixture proportions of concretes

Table 3 Relative mass loss of bars with respect to their initial weight. Bars are extracted from concretes with W/B of 0.55 after corrosion test with a duration of 32 days.

Table 4. Atomic Fe/Cl ratio of corrosion products: empty cells signify that the associated corrosion product is not observed in the concrete.

List of Figures:

Fig. 1 – Particle size distribution of materials using laser granulometry.

Fig. 2 – Experimental setup for accelerated corrosion test.

Fig. 3 – Compressive strength vs time in 100% relative humidity room for concrete with a W/B ratio of 0.4.

Fig. 4 – Compressive strength vs time in 100% relative humidity room for concrete with a W/B ratio of 0.55.

Fig. 5 – Coulomb charge of concretes with a W/B ratio of 0.4 vs curing time curing.

Fig. 6 – Coulomb charge of concretes with a W/B ratio of 0.55 vs curing time.

Fig. 7 – Comparison between chloride ion penetration obtained with ASTM C1202²⁷ and the coefficient of apparent chloride ions diffusion obtained with the method recommended by AFGC²⁸

Fig. 8 – Corrosion accelerated test. Monitoring of electrical current in steel bars placed at 0.8 inch (20 mm) from the saline solution

- 1 **Fig. 9 – Time taken to detect of corrosion depending on the distance between steel bars**
2 **and saline solution in concrete for W/B of 0.4 (a) and W/B of 0.55 (b).**
- 3 **Fig. 10 – Porosity accessible to water (AFGC 2007²⁸) and durability (AFGC 2004³³)**
- 4 **Figure 11 – SEM micrographs and EDS spectra of a) nested flower-like and b) lamellar-**
5 **like corrosion products observed in OPC 0.55.**
- 6 **Figure 12 – SEM micrographs and EDS spectra of gel-like corrosion product observed**
7 **in GP 0.55.**
- 8 **Figure 13 – SEM micrographs and EDS spectra of a) gel-like material and globular-like**
9 **and b) of hexagonal crystal-like corrosion products in AFA 0.55.**
- 10 **Figure 14 – SEM micrographs and EDS spectra of a) gel-like and globular-like, b)**
11 **nested needle-like and c) lamellar-like in LF 0.55.**
- 12

1

2 **Table 1 Chemical and physical analysis of materials (% by mass).**

Oxide	OPC	AFA	LF	GP
SiO ₂	20.3	26.00	18.4	71.80
Al ₂ O ₃	4.68	15.60	4.35	1.55
Fe ₂ O ₃	2.78	2.32	2.50	0.38
CaO	63.80	41.60	62.4	11.10
MgO	1.98	2.23	1.84	1.23
K ₂ O	0.82	0.75	0.65	0.52
Na ₂ O	0.23	0.84	0.22	12.90
SO ₃	3.33	3.71	2.98	--
LOI	2.61	3.30	7.25	0.04
D ₅₀ , μm	25.8	74.5	15.2	12.3
Blaine, ft ² /lb (m ² /kg)	1,904 (390)	5,224 (1070)	2,470 (506)	2,148 (440)
BET, ft ² /lb (m ² /kg)	6,103 (1,250)	16,941 (3,470)	7,811 (1,600)	3,222 (660)
Pozzolanic activity*, grains	--	36	--	418
Ca(OH) ₂ /oz (mgCa(OH) ₂ /g)	--	(82)	--	(955)

3 * *Modified Chapelle test*²⁹4 **Table 2 Mixture proportions of concretes.**

Mix labels	Binder (%) lb/lb (g/g)	W/B	Composition, lbs/yd ³ (kg/m ³)					Fresh concrete properties	
			Binder	Sand (0-5 mm) (0-1/4")	Fine aggregate (5-14 mm) (1/4-1/2")	Coarse aggregate (10-20 mm) (3/8-3/4")	Water	Air Entrained (%)	Slump, inches (mm)
OPC-0.4	100%OPC	0.4	651 (400)	1105 (679)	1394 (856)	348 (214)	260.2 (160)	7.4	7.4 (185)
OPC-0.55	100%OPC	0.55	570 (350)	1040 (639)	1394 (856)	348 (214)	313.8 (192.5)	6.6	7.2 (180)
GP-0.4	80% OPC 20% GP	0.4	651 (400)	1079 (663)	1394 (856)	348 (214)	260.2 (160)	6.6	8.8 (220)
GP-0.55	80% OPC 20% GP	0.55	570 (350)	1018 (625)	1394 (856)	348 (214)	313.8 (192.5)	6.4	7.2 (180)
AFA-0.4	80% OPC 20% AFA	0.4	651 (400)	1099 (675)	1394 (856)	348 (214)	260.2 (160)	5.0	7.2 (180)
AFA-0.55	80% OPC 20% AFA	0.55	570 (350)	1032 (634)	1394 (856)	348 (214)	313.8 (192.5)	6.6	7.2 (180)
LF-0.4	10% LF	0.4	651 (400)	1104 (678)	1394 (856)	348 (214)	260.2 (160)	7.2	8.2 (205)
LF-0.55	10% LF	0.55	570 (350)	1039 (638)	1394 (856)	348 (214)	313.8 (192.5)	6.2	7.4 (185)

5

6 **Table 3. Relative mass loss of bars with respect to their initial weight. Bars are extracted from concretes**
7 **with W/B of 0.55 after corrosion test with a duration of 32 days.**

Mass variation (%)	Concretes			
	OPC	LF	GP	AFA
	-22.8	-22.6	-9.4	-31.6

8

9

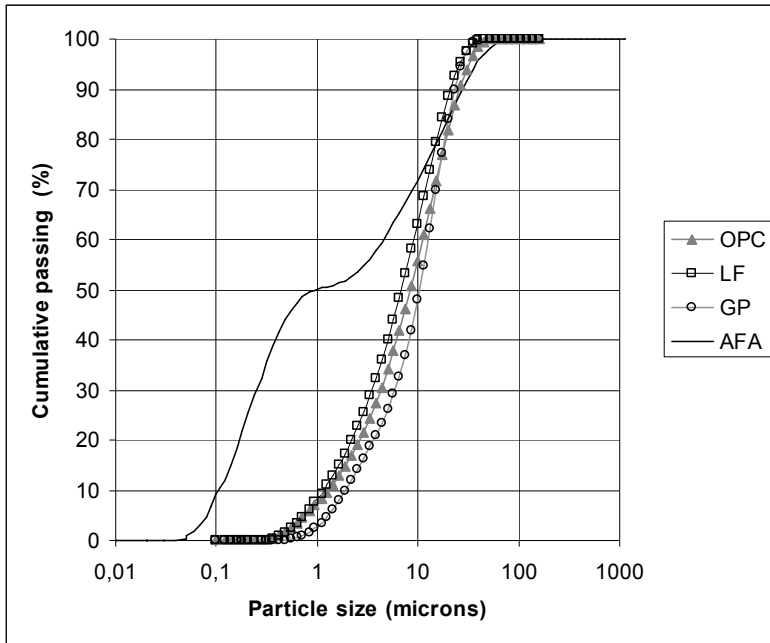
10

1

2 **Table 4. Atomic Fe/Cl ratio of corrosion products: empty cells signify that the associated corrosion**
3 **product is not observed in the concrete.**

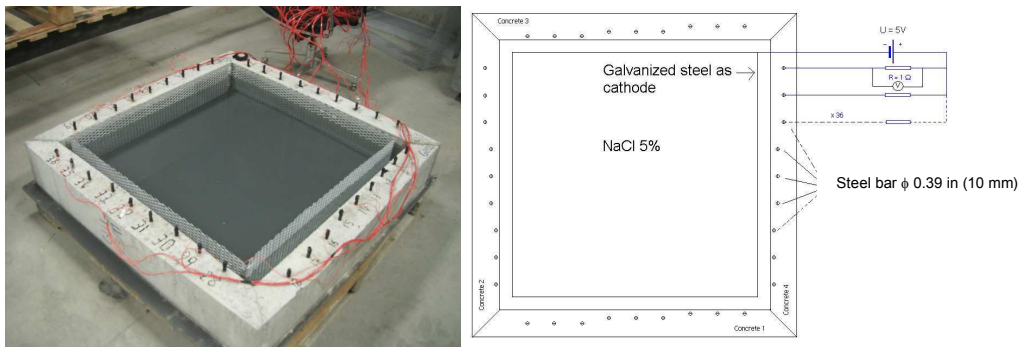
Concretes	Morphology of the corrosion products						
	Nested flower	Lamellar	Gel	Hexagonal crystal	Globular	Gel-globular	Nested needle
OPC 0.55	2.1	1.8					
GP 0.55			12.3				
AFA 0.55				1.3		2.2	
LF 0.55		2.6	8.0		2.7		1.2

4



1
2
3

Figure 1 Particle size distribution of materials using laser granulometry.



4
5
6

Figure 2 Experimental setup for accelerated corrosion test.

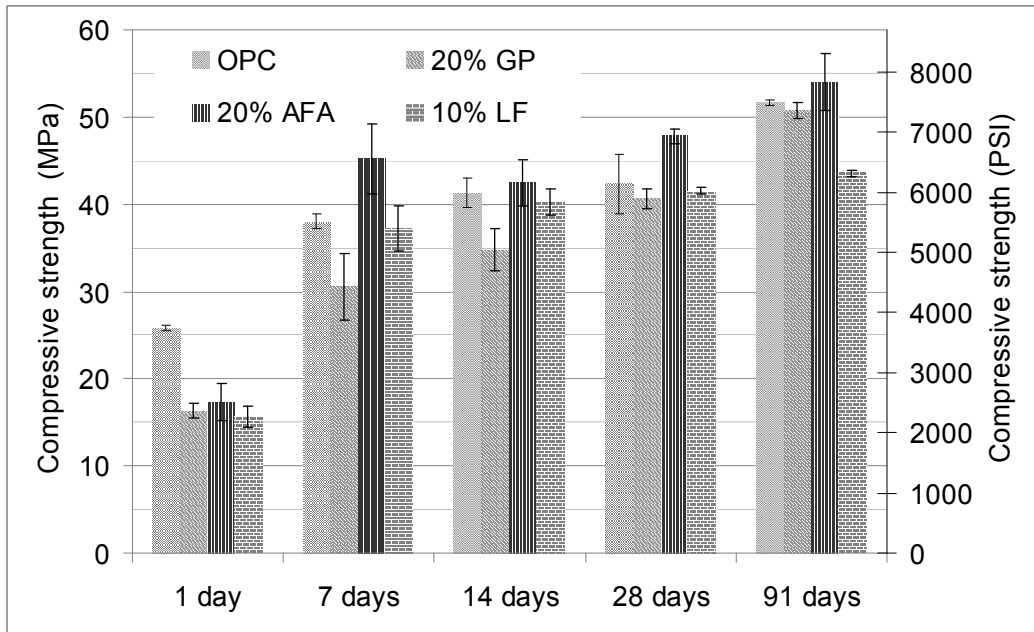


Figure 3 Compressive strength vs curing time for concretes with a W/B ratio of 0.4.

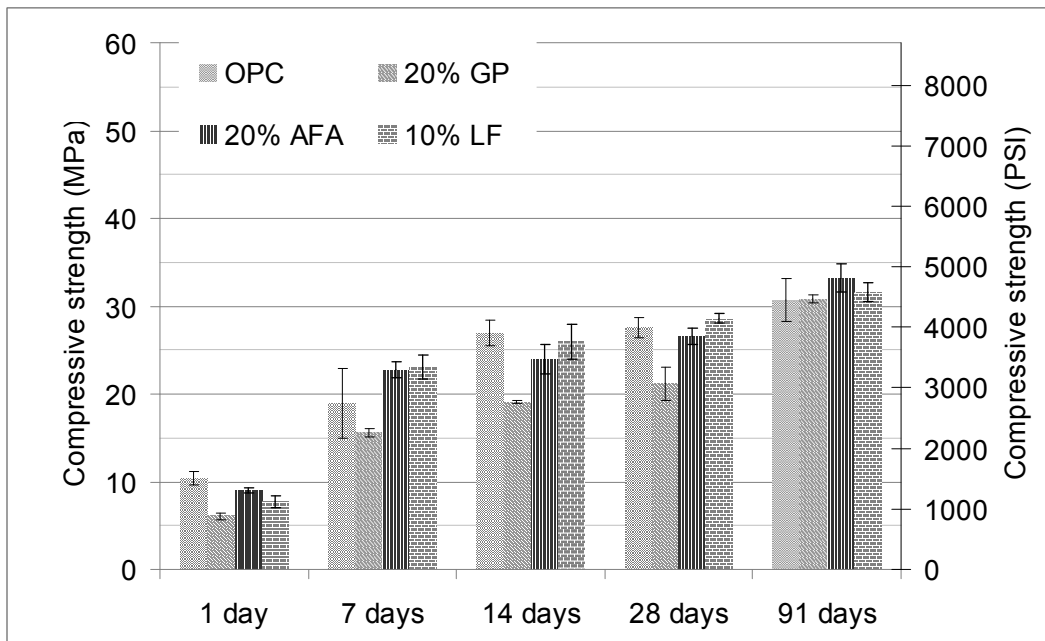


Figure 4 Compressive strength vs curing time for concretes with a W/B ratio of 0.55.

1
2
3

4
5
6
7

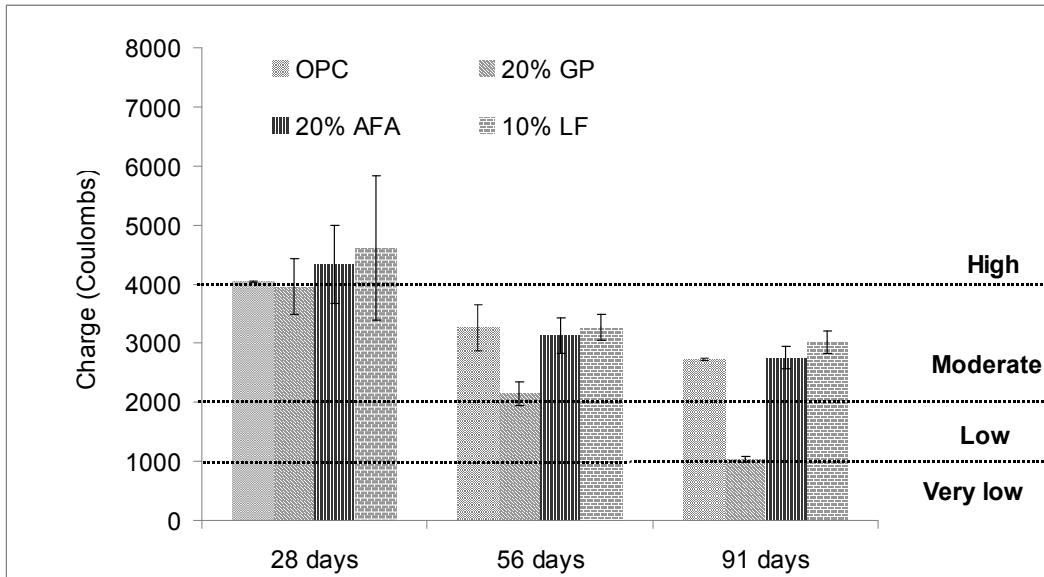


Figure 5 Chloride ion penetration of concretes with a W/B ratio of 0.4 vs curing time.

1
2
3
4
5

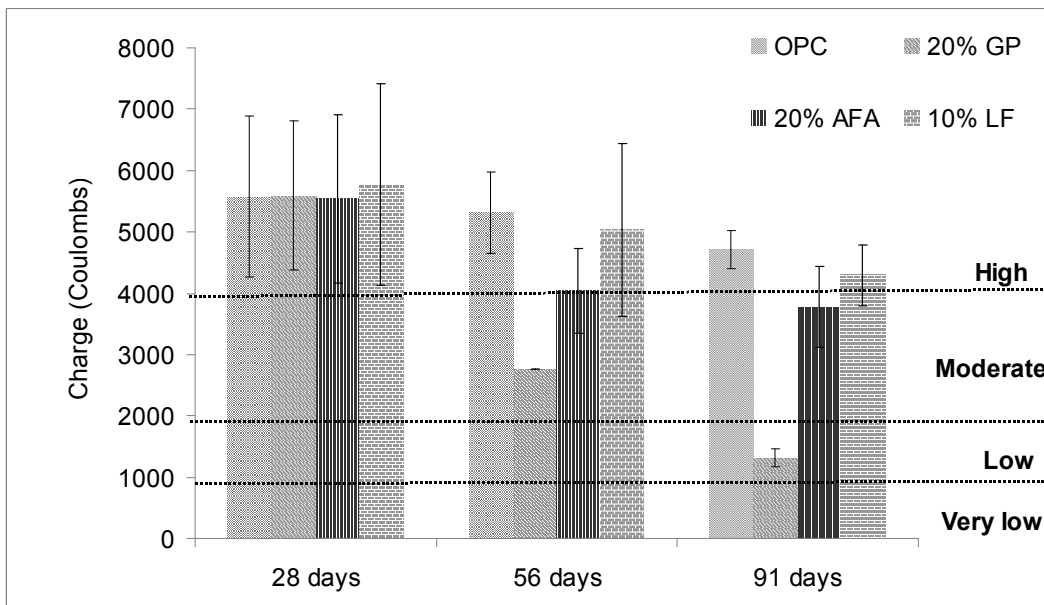
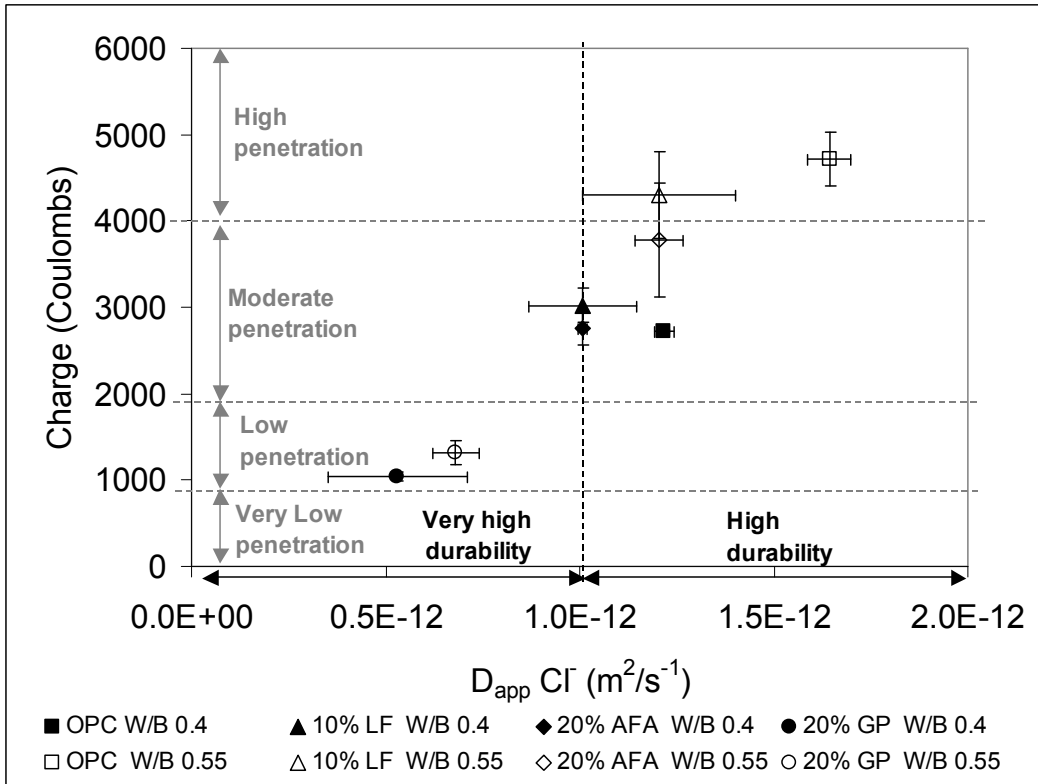


Figure 6 Chloride ion penetration of concretes with a W/B ratio of 0.55 vs curing time.

6
7
8
9
10



1

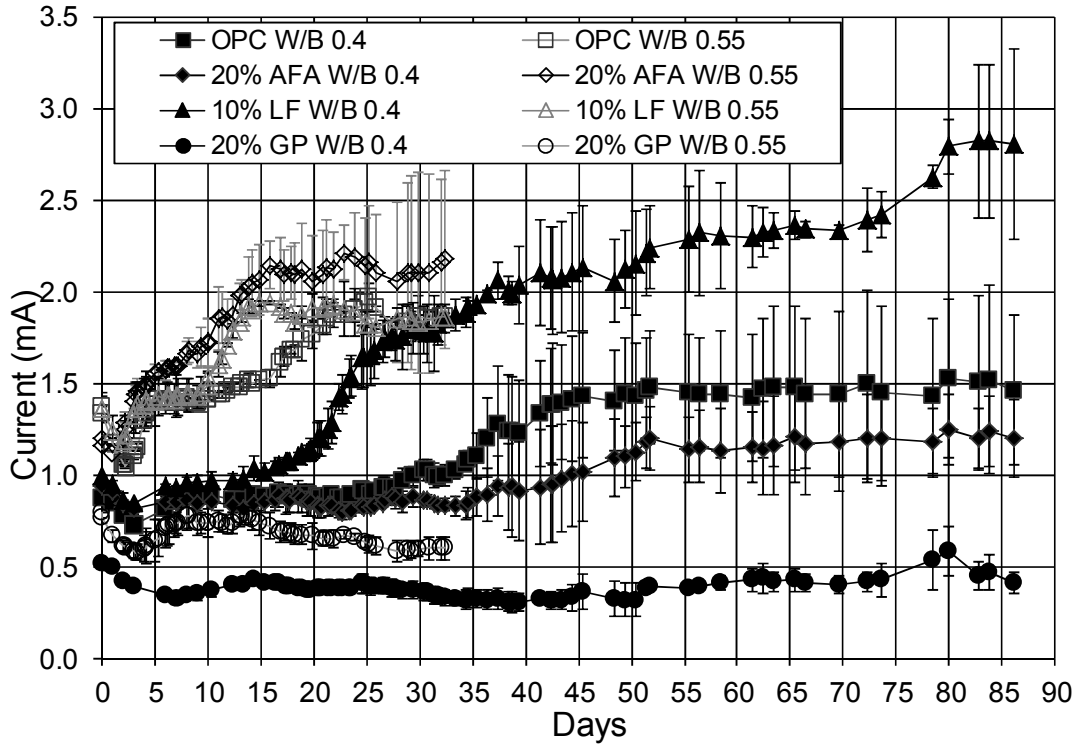
2

3

4

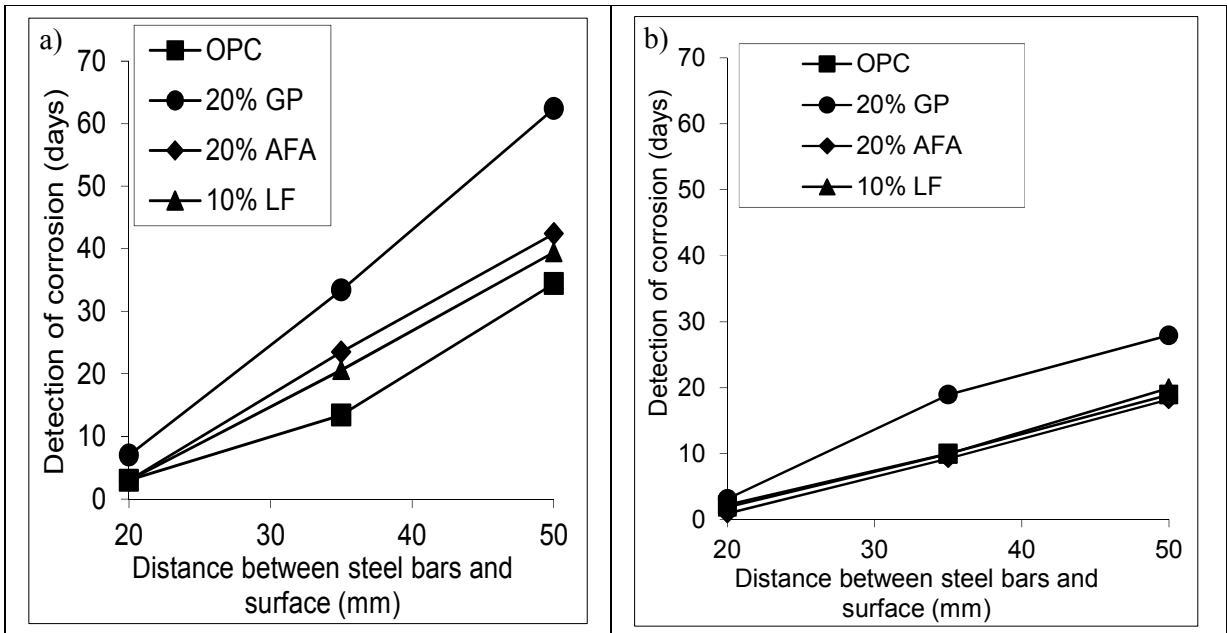
5

Figure 7 Comparison between chloride ion penetration obtained with ASTM C1202²⁷ and the coefficient of apparent chloride ions diffusion obtained with the method recommended by AFGC²⁸.



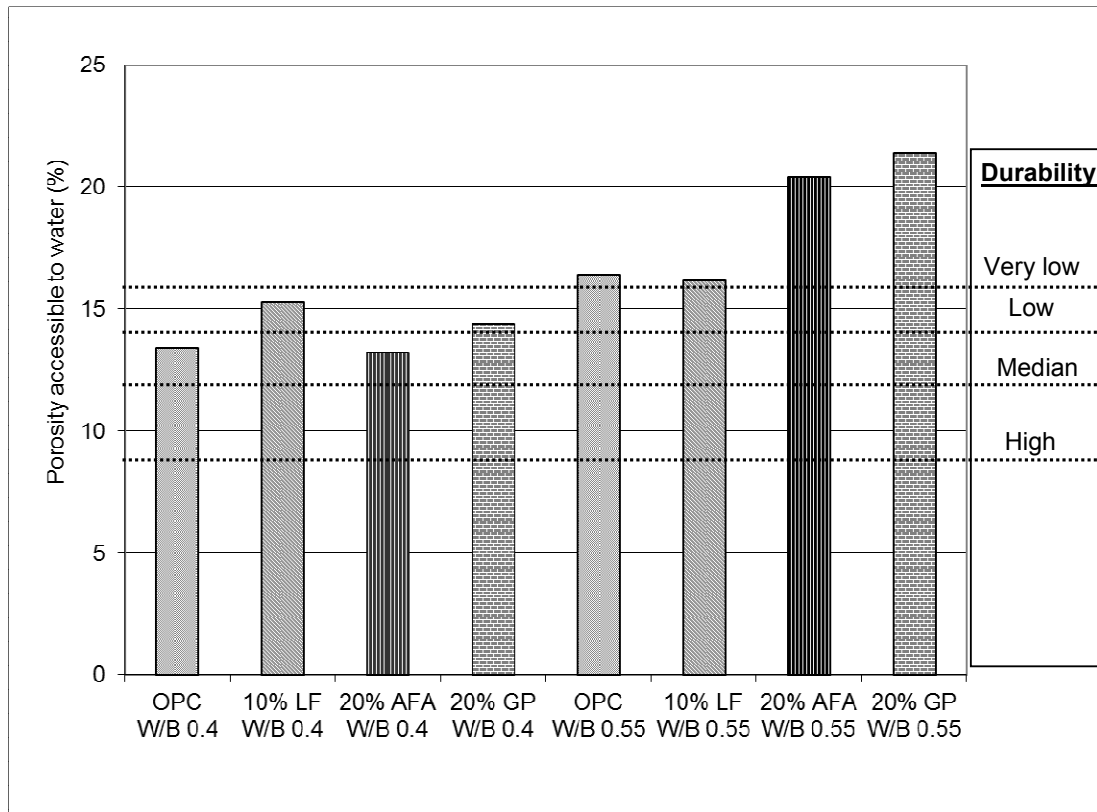
1
2
3
4

Figure 8 Corrosion accelerated test. Monitoring of electrical current in steel bars placed at 0.8 inch (20 mm) from the saline solution.



5
6

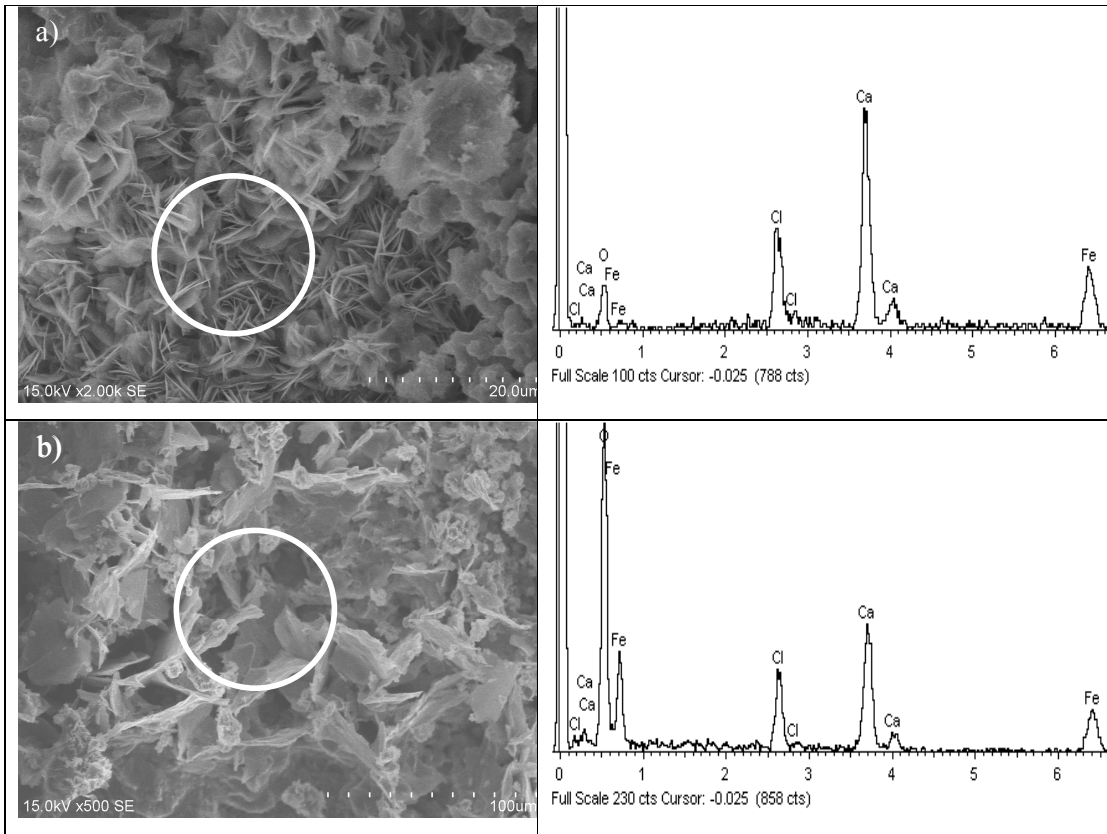
Figure 9. Time taken to detect of corrosion depending on the distance between steel bars and saline solution in concrete for W/B of 0.4 (a) and W/B of 0.55 (b)



1
2
3
4

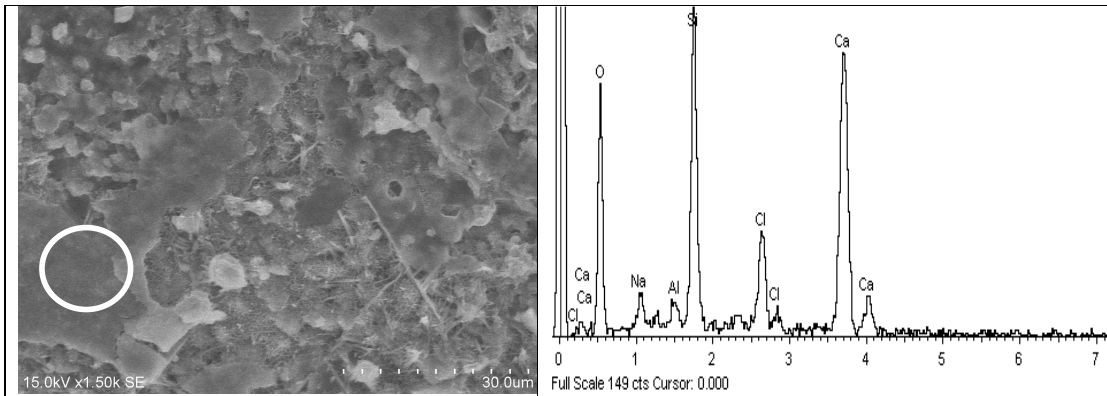
Figure 10. Porosity accessible to water (AFGC 2007²⁸) and durability (AFGC 2004³³)

1



2 **Figure 11. SEM micrographs and EDS spectra of a) nested flower-like and b) lamellar-like corrosion**
3 **products observed in OPC 0.55.**

4



5 **Figure 12. SEM micrographs and EDS spectra of gel-like corrosion product observed in GP 0.55.**

6

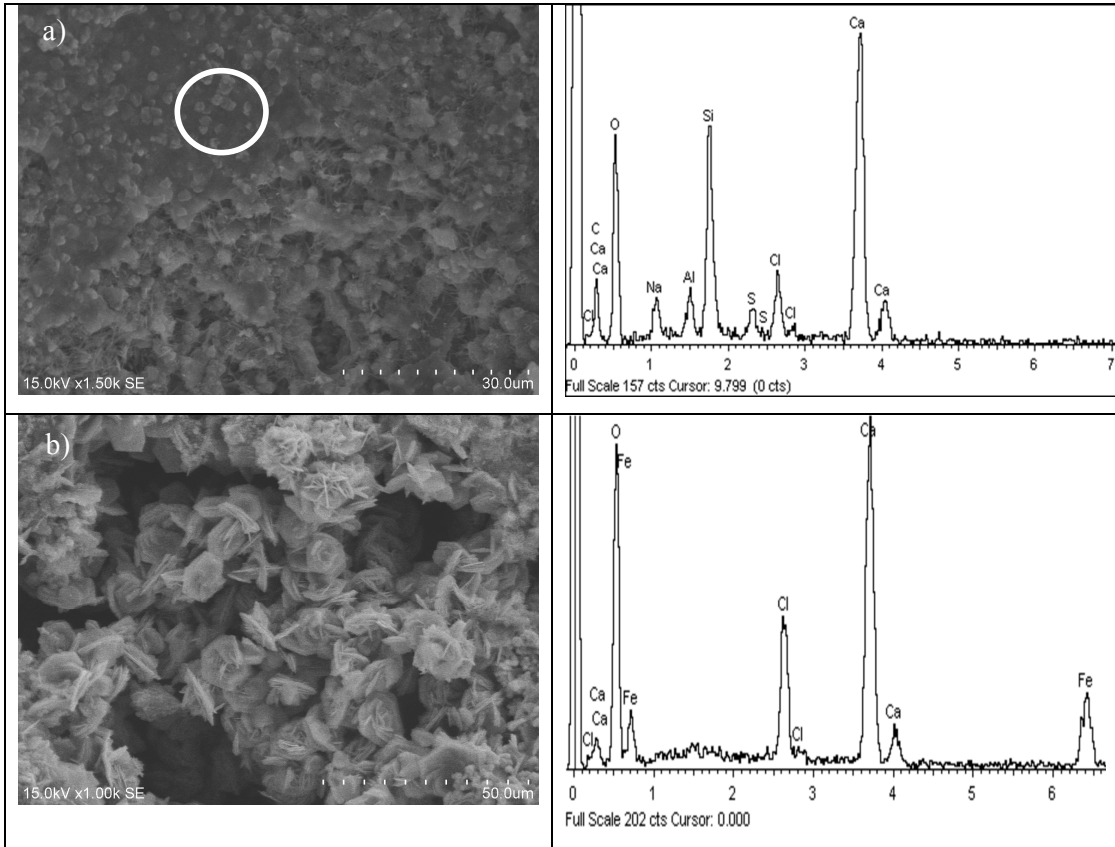
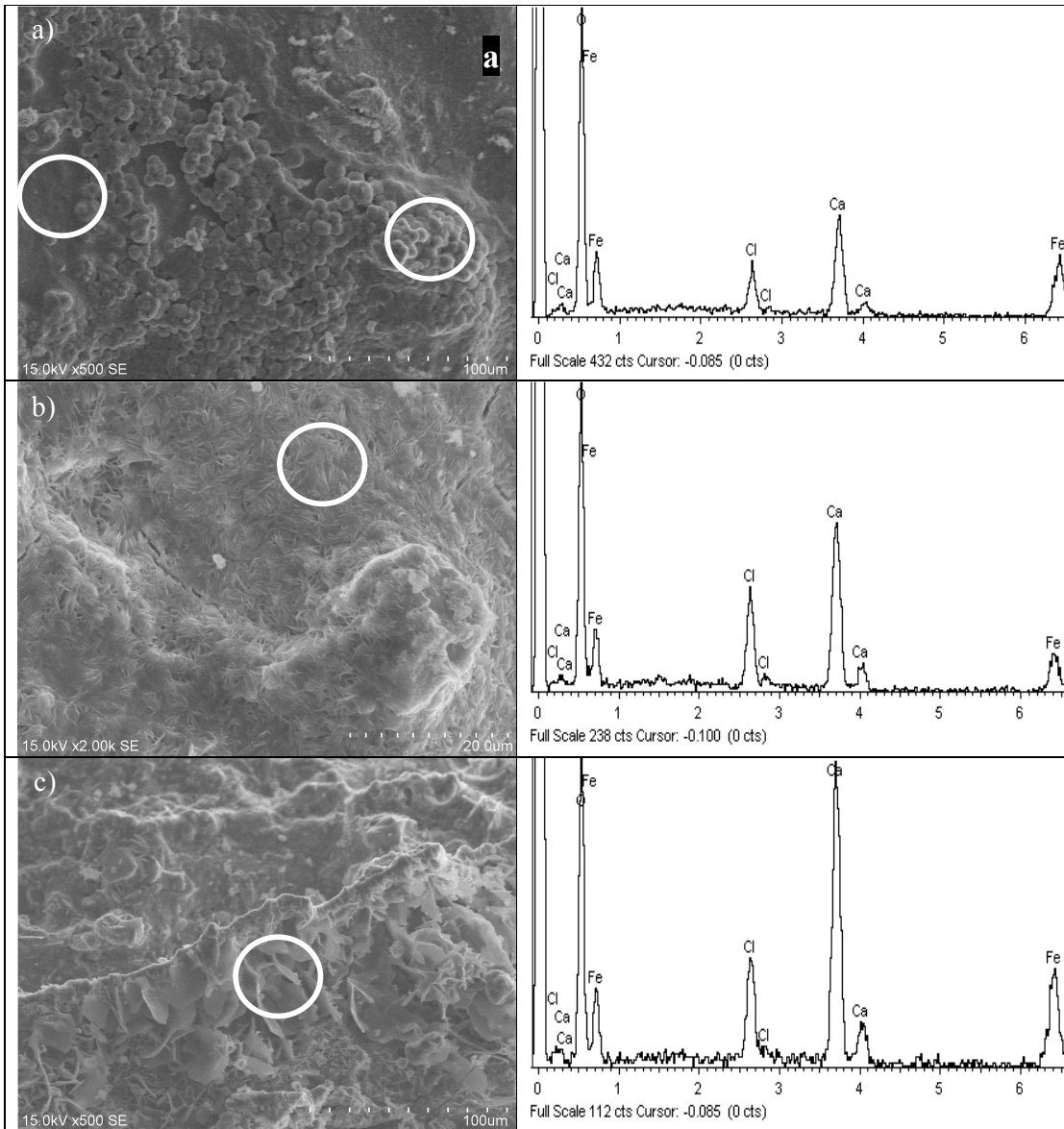


Figure 13. SEM micrographs and EDS spectra of a) gel-globular-like material and b) of hexagonal crystal-like corrosion products in AFA 0.55.

1
2
3
4

1



2 **Figure 14. SEM micrographs and EDS spectra of a) gel-like and globular-like, b) nested needle-like and c)**
3 **lamellar-like in LF 0.55.**

4